Front. Med. 2023, 17(6): 1204−1218
https://doi.org/10.1007/s11684-023-1007-9

RESEARCH ARTICLE

GID complex regulates the differentiation of neural stem cells by destabilizing TET2

Meiling Xia[1,2], Rui Yan[2], Wenjuan Wang[2], Meng Zhang[2], Zhigang Miao[2], Bo Wan (✉)[2], Xingshun Xu (✉)[1,2,3]

[1]Department of Neurology, The First Affiliated Hospital of Soochow University, Suzhou 215006, China; [2]Institute of Neuroscience, Soochow University, Suzhou 215006, China; [3]Jiangsu Key Laboratory of Neuropsychiatric Diseases, Soochow University, Suzhou 215123, China

Abstract **Brain development requires a delicate balance between self-renewal and differentiation in neural stem cells (NSC), which rely on the precise regulation of gene expression. Ten-eleven translocation 2 (TET2) modulates gene expression by the hydroxymethylation of 5-methylcytosine in DNA as an important epigenetic factor and participates in the neuronal differentiation. Yet, the regulation of TET2 in the process of neuronal differentiation remains unknown. Here, the protein level of TET2 was reduced by the ubiquitin-proteasome pathway during NSC differentiation, in contrast to mRNA level. We identified that TET2 physically interacts with the core subunits of the glucose-induced degradation-deficient (GID) ubiquitin ligase complex, an evolutionarily conserved ubiquitin ligase complex and is ubiquitinated by itself. The protein levels of GID complex subunits increased reciprocally with TET2 level upon NSC differentiation. The silencing of the core subunits of the GID complex, including WDR26 and ARMC8, attenuated the ubiquitination and degradation of TET2, increased the global 5-hydroxymethylcytosine levels, and promoted the differentiation of the NSC. TET2 level increased in the brain of the *Wdr26*$^{+/-}$ mice. Our results illustrated that the GID complex negatively regulates TET2 protein stability, further modulates NSC differentiation, and represents a novel regulatory mechanism involved in brain development.**

Keywords TET2; GID complex; neural stem cells; differentiation of neurons

Introduction

Ten-eleven translocation (TET) enzymes are important epigenetic factors that modulate gene transcription by hydroxylating DNA 5-methylcytosine (5mC) to 5-hydroxymethylcytosine (5hmC) for demethylation [1–3]. Although TET1, TET2, and TET3 share similar enzymatic actions, they differ in spatiotemporal expression patterns and nonredundant roles in gene expression, development, and diseases [4–6]. For example, TET1 and TET2 are highly expressed in embryonic stem cells (ESCs) [4,5], and TET3 is increasingly expressed during mouse development [6]. Among the three TET members, TET2 is involved in the pathological and physiological processes of the central nervous system (CNS), such as neurogenesis [7], depression [8], and Alzheimer's disease [9]. The TET2-FOXO3A axis participates in the regulation of neurogenic gene expression in neural stem cells (NSC) during adult neurogenesis [7], and TET2 knockdown affects neuronal survival [10]. These findings imply the critical role of TET2 in the CNS.

Although many studies have mainly focused on the function of TET2 and its 5hmC catalytic activity in DNA [1], issues about the regulation of TET2 itself still need to be addressed [11]. TET2 is regulated by specific factors at the transcriptional, translational, and post-translational levels in different processes. For instance, approximately 30 miRNA molecules, including miR-7, miR-125b, miR-29b/c, miR-26, miR-101, miR142, and Let-7, repress TET2 expression, and regulate malignant hematopoiesis [12]. TET2 is positively regulated by OCT4 upon the differentiation of mouse ESCs [4]. High glucose levels impede AMPK-mediated phosphorylation TET2 at serine 99, destabilizing TET2 and dysregulating the tumor suppressive function of TET2 [13]. IDAX (the inhibitor of disheveled and axin), which has been implicated in malignant renal cell carcinoma and colonic villous

Received December 6, 2022; accepted April 27, 2023

Correspondence: Xingshun Xu, xingshunxu@suda.edu.cn;
Wan Bo, wanbo@suda.edu.cn

adenoma, downregulates TET2 protein through caspase activation [14]. HIV-1 including viral protein R enhances viral replication by degrading TET2 and sustaining IL-6 expression through polyubiquitylation [15]. Calpain 1, a member of calcium-dependent protease family, mediates TET2 degradation and affects global 5hmC level and the expression of certain lineage-specific genes in mESCs [11]. However, the regulation of TET2 in neural differentiation is unclear.

Most members of the glucose-induced degradation-deficient (GID) complex have potential interactions with TET2 according to the mass spectrometry results. The GID ubiquitin ligase was initially found to regulate the polyubiquitin degradation of the key enzyme fructose-1,6-bisphosphatase from gluconeogenesis to glycolysis in yeast [16] and is essential for maintaining normal cell proliferation [17]. The major subunits of the human GID complex through comparative proteomics include RANBP9 (GID1), RMND5A (GID2), C17ORF29 (GID4), ARMC8 (GID5), WDR26 (GID7), TWA1 (GID8), MAEA (GID9), MKLN1, and RANBP10. Patients with *Wdr26* mutation show signs of mental retardation, speech retardation, and epilepsy [18]. It is a plasma-derived candidate biomarker for patients with depression [19]. Autism spectrum disorder is associated with the methylation level of *Armc8* [20]. GID4 can identify the substrate and activate the ubquitin ligase [21], and ARMC8 is necessary for GID4 binding [17]. Hence, it is of great interest to interrogate the possible function of GID complex to TET2 in the CNS.

Here, we demonstrated that the protein level of TET2 decreased in contrast to mRNA levels during the differentiation of NSC. The GID complex interacted with TET2 and regulated the stability of TET2 protein during the differentiation of NSC, subsequently influencing the level of DNA 5hmC, regulating the differentiation direction of NSC, and participating in the fate determination of NSC.

Materials and methods

Reagents, antibodies, cell lines, and oligos

Lists of the reagents, antibodies, cell lines, and oligos used in this study are provided in the Supplemental Material.

Animals

All animal procedure protocols were approved by the ethical committee of Soochow University. C57BL/6 mice (25.0–30.0 g, 8–12 weeks old) were purchased from Shanghai Research Center for Model Organisms. *Tet2*$^{flox/flox}$ line was obtained from the Jackson Laboratory (stock number 017573, B6; 129S4-Tet2tm1.1laai/J). These floxed mutant mice possess loxp sites flanking the exon 3 of the *Tet2* gene. Nestin-*Cre* mice were obtained from the Jackson Laboratory (stock number 003771, B6. Cg-Tg (Nes-*Cre*) 1 Kln/J). The *Tet2* conditional knockout (cKO) mice were generated by crossing loxp-flanked *Tet2* mice with Nestin-*Cre* mice. *Wdr26*$^{+/-}$ (C57BL/6) mice (stock number: KOAIP211129DY1) were generated by the CRISPR/Cas9 technology (Cyagen Biosciences Inc. Suzhou, China). Briefly, Cas9 mRNA and sgRNAs targeting the exons 2 and 3 of the mouse *Wdr26* gene were generated by *in vitro* transcription and then microinjected into the fertilized eggs from C57BL/6 mice for knockout mouse production. The founder mice were confirmed by genotyping and DNA sequencing analysis, and positive founders were bred to the next generation. The mice were housed in groups of one to five per cage and subjected to a standard 12 h light–12 h dark cycle in a room maintained at 24 ± 2 °C with free access to water and chow. The morning of vaginal plug detection was designated as embryonic day (E) 0.

Cell culture, transfection, and differentiation

Mouse neuro2a neuroblastoma (N2a) cells, mouse hippocampal neuronal (HT22) cells, and human embryonic kidney (HEK293t) cells were cultured in Dulbecco's modified eagle medium (DMEM) supplemented with 10% fetal bovine serum (FBS). The cells were cultured in a humidified incubator at 37 °C with 5% CO_2. For transfection, HEK293t cells were transfected at 70% confluency by using polyethyleneimine (PEI), and N2a cells were transfected at 70% confluency by using a PL transfection reagent according to the instructions. For differentiation induction, the N2a cells were induced by adding 20 μmol/L retinoic acid in DMEM supplemented with 1% FBS for 12 h.

Isolation, culture, transfection, and induced differentiation of neural stem cells

NSC were isolated from the dentate gyrus (DG) region of E14.5 mice and were cultured in DMEM/F12 supplemented with 2% B27, 20 ng/mL basic fibroblast growth factor, and 20 ng/mL epidermal growth factor (EGF). The NSC from each fetal mouse were cultured separately, and their genotypes were identified by tails individually. The primary neurosphere was cultured 5 days before experiment, and then neurosphere-derived single cells were inoculated into untreated 12-well plates at a density of 1×10^6 cells/mL. For NSC transfection, the cells were transfected with a lipofectamine stem transfection reagent according to the manufacturer's protocol. The plates were coated with 10 μg/mL polyornithine (PLO) and 5 μg/mL laminin for 1 day each before the induction of differentiation. The NSC were digested with accutase and inoculated into a coated plate

at a density of 1 × 10^6 cells/mL. The growth medium containing 1 μmol/L forskolin and 1 μmol/L retinoic acid was changed after 24 h. NSC-induced differentiation was induced and stopped after 48 h.

Primary neuron and astrocyte isolation and culture

The plates were coated with 0.1 mg/mL poly-D-lysine at 37 °C overnight before neuron isolation. Brain tissues were isolated from day 16 embryos, and the meninges were removed under a microscope. The tissues were digested with 0.125% trypsin at 37 °C for 10 min, and the reaction was terminated with DMEM supplemented with 10% FBS. The suspension was filtered with a 40 μm filter and centrifuged at 1000 rpm for 5 min. The cell precipitate was resuspended in the neurobasal medium supplemented with 2% B27 and 0.5 mmol/L L-glutamine. Neurons were cultured for 7 days, and half of the medium was replaced with fresh medium every 3.5 days.

For astrocyte isolation, the brains of the 2-day-old mice were removed, and the meninges were removed under a microscope. The tissue was trypsinized with 0.25% trypase at 37 °C and dissociated, and then the cells were plated in a DMEM containing 10% FBS. After 24 h, the culture medium was changed to a fresh DMEM containing 10% FBS. The culture medium was changed every 3 days. The cells were subcultured and purified on the 5th day at 85% confluency. After 10 days of cell growth, the cells were inoculated into the well plate for the follow-up experiment.

Immunoprecipitation (IP), protein extraction, and Western blot

For endogenous immunoprecipitation (IP), N2a cells at 70% confluency in three 90 mm dishes were lysed in 1 mL RIPA buffer (50 mmol/L Tris, pH 8.0; 0.1% SDS; 150 mmol/L NaCl; 1 mmol/L EDTA, pH 8.0; 1 mmol/L EGTA, pH 8.0; 0.5% deoxycholate, and 1% TritonX-100) containing 100× cocktail and 200× DTT at 4 °C under rotary agitation for 2 h. Approximately 5% input was obtained through 30 min of centrifugation at 13 200 rpm at 4 °C. Total protein was divided into two groups, and each group was not less than 2 mg. The protein supernatant was added after agarose beads were activated and were pre-cleared by rotating on the rotator for 2 h at 4 °C. The supernatant was moved to a new tube, and the same amounts of TET2 and IgG antibodies were added to the two tubes, which were then rotated at 4 °C overnight. The supernatant was transferred to the agarose beads and rotated at 1000 rpm at 4 °C for 15 h. The supernatant was removed after 3 min of centrifugation at 1000 rpm and 4 °C. A 2× loading buffer (50 μL) was added to the precipitate, and the samples were boiled at 95 °C for 10 min.

For exogenous IP, HEK293t cells were transiently transfected with target plasmids by using PEI. Three 90 mm dishes of HEK293t cells were used as one group. HA-WDR26 + VECTOR, HA-WDR26 + FLAG-TET2 (HA-ARMC8 + VECTOR, HA-ARMC8 + FLAG-TET2) were transfected for 48 h separately. Cell pellets were lysed with a lysis buffer (150 mmol/L NaCl; 25 mmol/L Tris-HCl, pH7.4; 10% glycerol; 0.5% TritonX-100; 2 mmol/L $MgCl_2$) containing 100× cocktail and 200× DTT at 4 °C for 3 h. After 30 min of centrifugation at 4 °C and 13 200 rpm, 60 μL of supernatant was collected as input. The rest was placed in FLAG beads and rotated at 4 °C for 11 h. The supernatant was removed by a magnetic shelf, and the beads were cleaned twice with lysis buffer. Loading buffer (2×, 50 μL) was added to the precipitate, and the samples were boiled at 95 °C for 10 min.

For total protein extraction, cell pellets were lysed using RIPA buffer containing 50 mmol/L Tris (pH 8.0), 0.1% SDS, 150 mmol/L NaCl, 1 mmol/L EDTA (pH 8.0), 1 mmol/L EGTA (pH 8.0), 0.5% deoxycholate, and 1% TritonX-100 on ice for 30 min. Then, 15 min of centrifugation was performed at 4 °C and 12 000 rpm. The supernatant was collected and boiled for 10 min at 95 °C after 1/4 volume of 5× loading buffer was added. Approximately 30 μg of the protein aliquot of each sample was separated using standard SDS-PAGE and transferred to a PVDF membrane. After the transfer, the PVDF membrane was blocked with 10% nonfat milk for 1 h at RT and incubated overnight at 4 °C with a target primary antibody. Immunoreactive bands were detected using an ECL chemiluminescence reagent after incubation with a secondary antibody for 1 h. The details of the antibody and reagents used in this experiment are listed in the Supplemental Material.

RNA isolation and quantitative RT-PCR

Total RNA was extracted using RNAiso plus and was reverse transcribed using a reverse transcription kit according to the manufacturer's protocol. Quantitative real-time PCR was performed using 2× SYBR Green PCR Master Mix with a 7500 Real-Time PCR system (Applied Biosystems, Foster City, CA, USA). GAPDH was used as an endogenous control for real-time PCR amplification. For data analysis, fold change was calculated using the $^{\Delta\Delta}$Ct method according to the threshold cycle value obtained from RT-PCR. The sequences of the primers used in this study are listed in the Supplemental Material.

Genomic DNA isolation and dot blot

Cell pellets were digested in 600 μL of DNA lysis buffer (100 mmol/L Tris-HCl, pH 8.5; 5 mmol/L EDTA; 0.2% SDS; 200 mmol/L NaCl) and mixed with 20 mg/mL

proteinase K, and incubated at 55 °C overnight. An equal volume of phenol:chloroform:isoamyl alcohol solution (25:24:1, saturated with 10 mmol/L Tris, pH 8.0, and 1 mmol/L EDTA) was added on the second day. The mixture was vortexed for 1 min and separated through centrifugation for 10 min at 12 000 rpm at 4 °C. The aqueous layer solution was transferred to a new tube and precipitated with 600 μL of isopropanol. DNA pellets were obtained through 15 min of centrifugation at 12 000 rpm and 4 °C and washed with 70% ethanol twice. The DNA was air dried and eluted with nuclease-free water.

For dot blot, a 20 μL system containing 2000 ng of DNA, 10 μL of 2 M NaOH, and double-distilled water was prepared and left to stand at 4 °C for 20 min. 2 μL of each sample was spotted onto a nitrocellulose (NC) membrane and let the membrane dry at room temperature (RT). DNA was fixed to the membrane by incubating at 80 °C for 30 min. Then the NC membrane was blocked with 10% nonfat milk for 1 h at RT and incubated with 5hmC or 5mC antibody overnight at 4 °C. Immunoreactive signal was detected by the ECL chemiluminescence reagent after incubating with the secondary antibody for 1 h. And the dot signal was quantified by ImageJ software.

Immunofluorescence

The samples were fixed overnight at 4 °C in 4% PFA in PBS for 30 min, treated with 0.3% Triton X-100 in PBS (PBST) for 10 min and then blocked with 5% BSA in 0.3% PBST for 1 h at RT. Subsequently, the samples were incubated with sample-specific primary antibodies overnight at 4 °C, washed three times with PBS, and incubated with florescent-labeled secondary antibody containing DAPI for 1 h at RT. The samples were imaged with a fluorescence microscope (Axio Scope A1, Zeiss) after patching on the microslide.

Construction of N2a knockout cell lines by CRISPR Cas9

The sgRNA was designed using Benchling. The oligos were then annealed according to a standard protocol and ligated into the vector lentiCRISPR v2 (Addgene, #52961) and confirmed by sequencing. The plasmids were transfected into the N2a cell line at 60% confluency by using a PL transfection reagent for 36 h. Puromycin was added to the culture for the selection of transfected cells for 48 h after transfection. The surviving cells were subjected to picking single clones by limiting dilution. The sequences of the oligos used in this study are provided in the Supplemental Material.

Statistical analysis

All statistical analyses were performed using Prism 7.0 (GraphPad Software) and expressed as mean ± SEM. *N* numbers were reported in figure legends. The differences with different treatments were determined by *t*-test or one-way ANOVA followed by Tukey's post hoc test. $P < 0.05$ was considered statistically significant.

Results

Proteasome pathway regulates the stability of TET2 in NSC

To investigate the function of *Tet2* in the progress of neural differentiation, we found that the expression levels of *Tet2* and DNA base 5hmC significantly decreased in the hippocampi of the *Tet2* conditional knockout (cKO) mice compared with the control mice, whereas levels of *Tet1* and *Tet3* did not change ($P < 0.01$, 0.001, Fig. S1A–S1D). Immunofluorescence analysis for neural markers showed decreased neurogenesis and the enhanced proliferative capacity of NSC in the DG region of the adult *Tet2* cKO mice and increased NSC self-renewal capacity in the neurospheres isolated from the *Tet2* cKO mice at E14.5 ($P < 0.05$, 0.01; Fig. 1). We further extracted NSC from wild-type (WT) mice and induced the differentiation of NSC. After NSC differentiation, the mRNA level of *Tet2* was upregulated ($P < 0.05$, Fig. 2A), whereas the protein level was downregulated ($P < 0.01$, Fig. 2B and 2C). To explore the reason for this inconsistency, we investigated the downregulation of TET2 after NSC differentiation. Given that the main pathways affecting the stability of TET2 include the caspase 3-dependent proteolytic cleavage pathway [14], calpeptin-mediated degradation [11], and proteasome-mediated ubiquitin degradation [22], we transfected HEK293t cells with FLAG-TET2 plasmids and then treated them with proteasome inhibitor (MG132), calcium protease inhibitor (calpeptin), and apoptosis inhibitor (Z-VAD-FMK) successively to detect their effects on the expression of FLAG-TET2. The results showed that treatment with MG132 significantly increased the expression of FLAG-TET2 ($P < 0.05$, Fig. 2D and 2E). Then, we treated the nerve cells, N2a cells and HT22 neuronal cells with the inhibitors. Similarly, MG132 significantly inhibited the degradation of endogenous TET2 in the N2a and HT22 cells ($P < 0.05$, 0.01, Fig. 2F–2I). These results indicated that proteasome-mediated degradation is the main pathway regulating the stability of TET2 in NSC.

TET2 interacts with the subunits of the GID complex

Previous study showed many TET2-interacting proteins in the mouse ESCs [23]. We further analyzed and identified that the proteins interacting with TET2 were proteins involved in RNA splicing, translation initiation

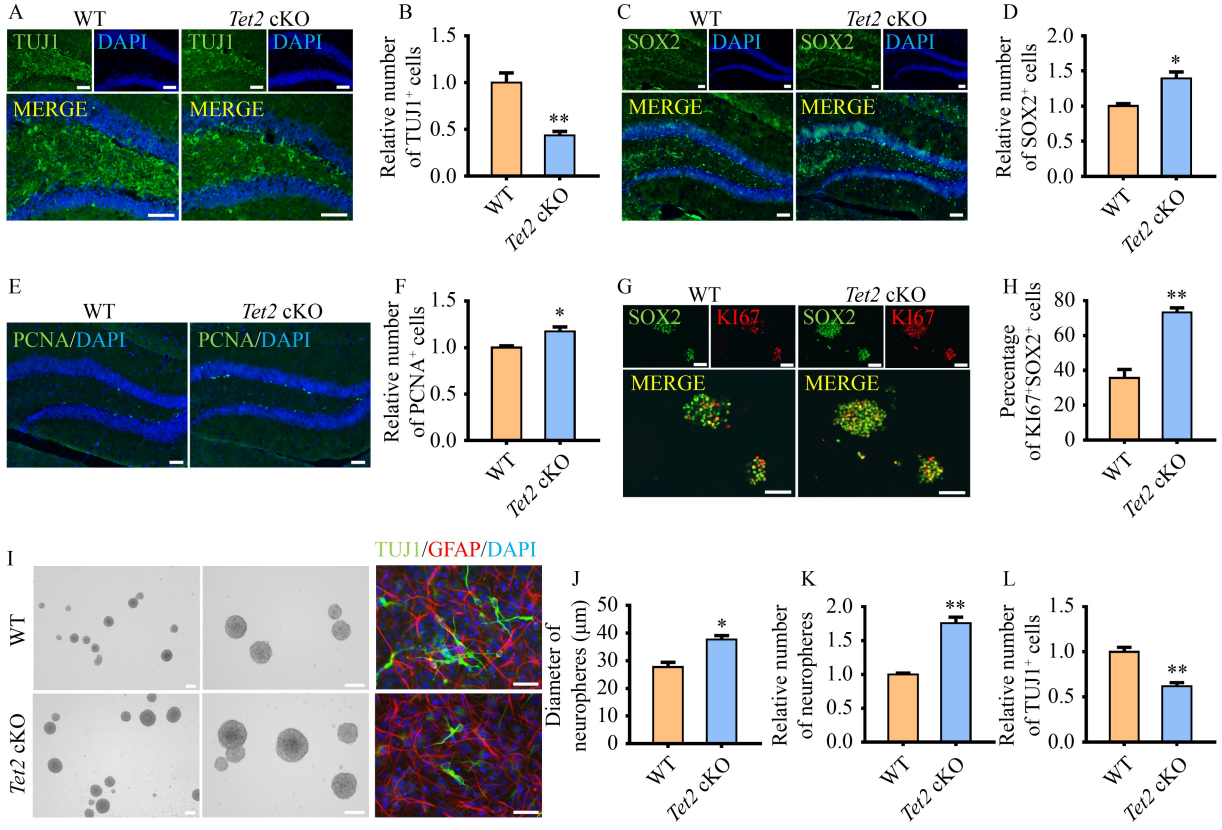

Fig. 1 Ablation of *Tet2* reduced the neural differentiation of NSC. (A,B) Representative immunofluorescence (IF) images (A) and relative quantification (B) of TUJ1$^+$ immature neurons (green) in the DG of 2-month-old wild-type (WT) and *Tet2* cKO mice. Scale bar, 50 μm; $n = 4$. (C,D) Representative IF images (C) and relative quantification (D) of SOX2$^+$ NSC (green) in the DG of 2-month-old WT and *Tet2* cKO mice. Scale bar, 50 μm; $n = 4$. (E,F) Representative IF images (E) and relative quantification (F) of PCNA$^+$ proliferating NSC (green) in the DG of 2-month-old WT and *Tet2* cKO mice. Scale bar, 50 μm; $n = 4$. (G,H) The neurospheres were extracted from E14.5-day-old WT and *Tet2* cKO mice. After 5 days of incubation, neurosphere-derived single cells were cultured for 5 days to detect the number and diameters of neurospheres. After neurosphere-derived single cells were plated, the growth medium containing forskolin (1 μmol/L) and retina acid (1 μmol/L) was used to induce the differentiation of the NSC for 48 h for IF staining. Representative IF images (G) and relative quantification (H) of SOX2$^+$KI67$^+$ proliferating neurospheres (yellow). (I) Representative bright-field images of the second passage hippocampal neurospheres culture *in vitro* on day 5 and IF images of TUJ1$^+$ immature neurons (green), and GFAP$^+$ astrocytes (red) of WT and *Tet2* cKO mice. Scale bar of bright-field images, 25 μm; scale bar of IF images, 50 μm; $n = 3$. (J,K) Quantification of the diameter (J) and relative number (K) of cultured neurospheres. (L) Quantification of relative TUJ1$^+$ neurons after NSC differentiation was induced. Quantified data were normalized to the control group. The value was equal to 1. All data were presented as mean ± SEM. Unpaired two-tailed Student's *t*-test was used. *$P < 0.05$; **$P < 0.01$.

pathway, and protein degradation (Fig. 3A and 3B). To identify the potential E3 ligase that may be involved in TET2 degradation, the proteins with potential interaction with TET2 were screened by cluster analysis. The members of the GID complex, including WDR26, ARMC8, MKLN1, RANBP10, RANBP9, and MAEA, were found to potentially interact with TET2 (Fig. 3C and 3D). Among the subunits of the GID complex, WDR26 is the central subunit of mammalian GID complex and acts as a scaffold protein for substrate recruitment in the E3 ubiquitin ligase complex [24]. ARMC8 is responsible for recruiting GID4 [25], an activator of E3 ligase activity, to enable efficient E2 enzyme binding and catalytic core orientation toward the substrate.

To verify the interaction between the GID subunits and TET2, we first cotransfected FLAG-TET2 plasmids with HA-WDR26/HA-ARMC8 (two core subunits of the GID complex) separately in HEK293t cells and confirmed the interaction between WDR26/ARMC8 and TET2 (Figs. 3E, 3F, S2A and S2B) by co-immunoprecipitation. To gain further insight into the association between TET2 and GID complex, we induced the immunoprecipitation of soluble N2a cell extracts with an anti-TET2 antibody and then performed Western blot analysis of the immunoprecipitated proteins with anti-WDR26 or anti-ARMC8 antibody and revealed the presence of WDR26 and ARMC8 in the anti-TET2 immunoprecipitates (Fig. 3G). These results showed a potential role of the GID complex with WDR26 and ARMC8 as key subunits in the proteasome system that may be involved in the regulation of protein stability of TET2.

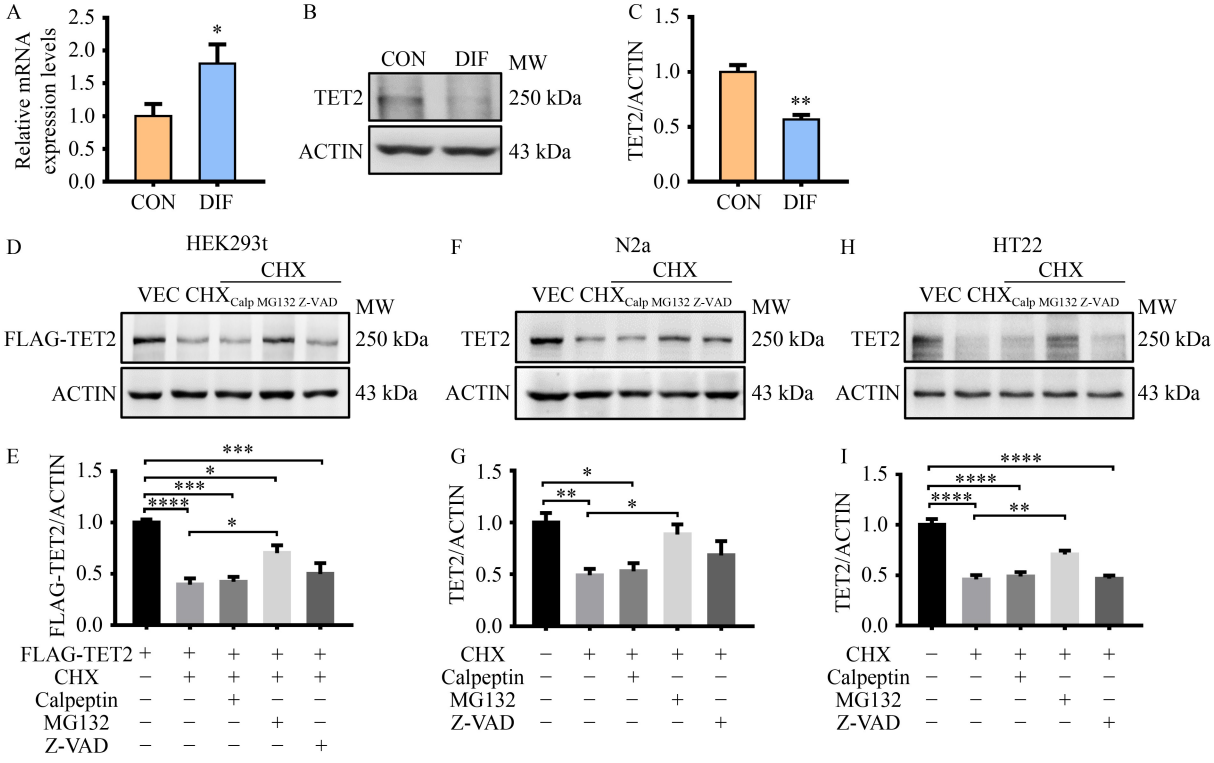

Fig. 2 Proteasome pathway is the main pathway that affects the stability of TET2. (A) The quantitative real-time PCR of *Tet2* level before and after NSC differentiation; $n = 5$. (B,C) Representative Western blots (B) and quantitative analysis of TET2 (C) level before and after NSC differentiation; $n = 4$. (D,E) Representative Western blots (D) and quantitative analysis of FLAG-TET2 (E) in HEK293t cells. HEK293t cells were transfected with FLAG-TET2 for 24 h and then treated with cycloheximide (CHX; 50 μg/mL) alone or in combination with MG132 (10 μmol/L), Z-VAD-FMK (10 μmol/L), or calpeptin (20 μmol/L) for 12 h. Cell lysates were subjected to Western blotting with the FLAG antibody; $n = 4$. (F–I) Representative Western blots (F,H) and quantitative analysis of TET2 (G,I) in N2a (F,G) or HT22 cells (H,I). N2a or HT22 cells were treated with CHX (15 μg/mL for HT22 cells and 25 μg/mL for N2a cells) alone or in combination with MG132 (10 μmol/L), or Z-VAD-FMK (10 μmol/L), or calpeptin (20 μmol/L) for 12 h. Cell lysates were subjected to Western blotting with the TET2 antibody; $n = 4$. Quantified data were normalized to the control group. The value was equal to 1. All data were presented as mean ± SEM. Unpaired two-tailed Student's *t*-test (A, C) and one-way ANOVA (E, G, I) were used. *$P < 0.05$; **$P < 0.01$; ***$P < 0.001$; ****$P < 0.0001$.

The protein levels of GID complex subunits rise reciprocally with TET2 level upon NSC differentiation

To explore the role of the GID complex in the CNS, we first extracted NSC, neurons from E14.5-day-old mice, and astrocytes from 2-day-old mice (Fig. 4A–4C). The expression of TET family members and GID complex members in the three kinds of neuronal cells were detected. RT-PCR results showed that the members of the TET family and GID complex showed similar expression patterns in different cells, that is, all of them were highly expressed in the neurons (Fig. 4D). After NSC differentiation, the mRNA level of *Tet2* was upregulated ($P < 0.05$, Fig. 5A), protein level was downregulated ($P < 0.01$, Fig. 5B and 5C). By contrast, the mRNA and protein levels of the GID complex members were all upregulated ($P < 0.05$, 0.01, Fig. 5A–5E). Consistently, after the differentiation of N2a cell, the mRNA level of *Tet2* was upregulated ($P < 0.05$, Fig. 5F) and the protein level was downregulated ($P < 0.05$, Fig. 5G and 5H). However, the mRNA and protein levels of GID complex core subunits were upregulated ($P < 0.05$, 0.01, Fig. 5F–5J). The expression levels of ARMC8 and WDR26 increased, whereas the expression level of TET2 decreased during N2a cell differentiation (Fig. 5K). The differentiation potential of the NSC decreased dramatically 2 weeks after the birth of the mice [26]. Accordingly, we extracted the hippocampal tissues of 1-, 7-, 14-, 21-, and 30-day-old littermates and observed changes in TET2, WDR26, and ARMC8 levels during brain development. The expression levels of WDR26 and ARMC8 increased with age, but the expression level of TET2 decreased gradually with age from the second week (Fig. 5L).

TET2 protein levels are directly regulated by the GID complex

To directly investigate the relationship between the GID complex and TET2 during neuronal differentiation and the role of the GID complex in the regulation of the stability of TET2, we generated *Armc8* KO, *Wdr26* KO,

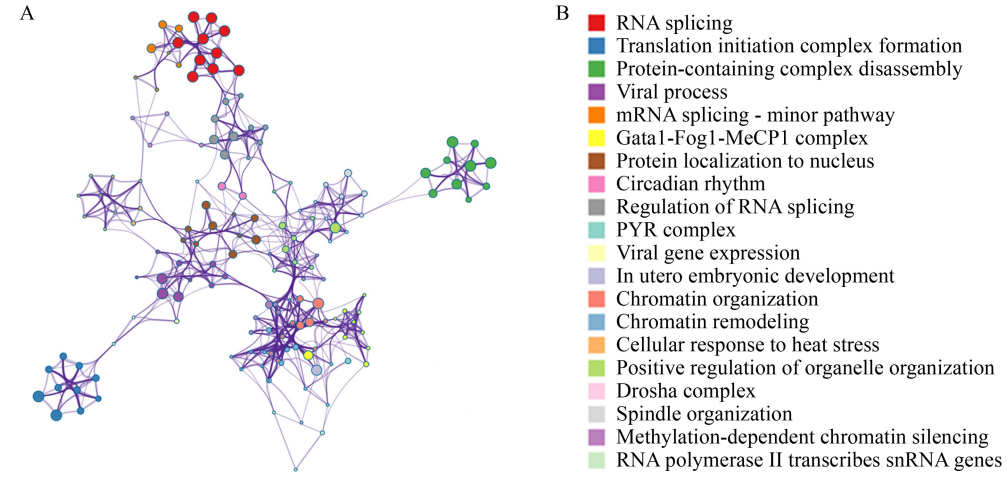

C

Symbol	#AAs	MW	TET2-IP	Ctrl-IP
ARMC8	673	75.3	23	2
RANBP10	648	70	8	
WDR26	514	58.5	12	2
MKLN1	735	84.8	5	
RANBP9	679	74.9	6	3
MAEA	396	45.3	4	2

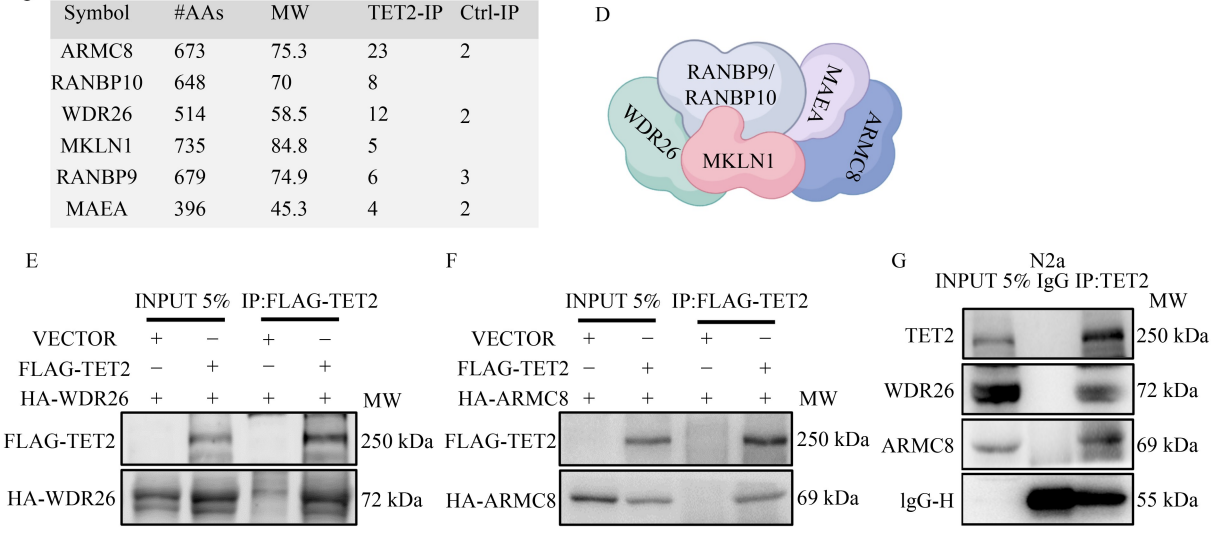

Fig. 3 TET2 interacts with GID complex subunits WDR26 and ARMC8. (A,B) Using the Metascape website for functional analysis based on the mass spectra of TET2 interacting proteins. (C,D) The list of GID complex subunits that could potentially interact with TET2 were sieved out by cluster analysis. Mouse FLAG-TET2 and HA-WDR26/HA-ARMC8 expression plasmids were co-transfected into HEK293t cells, and using anti-FLAG magnetic beads for extraneous immunoprecipitation. Co-immunoprecipitation (Co-IP) assays was used to validate interaction of HA-WDR26 (E) or HA-ARMC8 (F) with FLAG-TET2 in HEK293t cells. (G) Endogenous Co-IP experiments of TET2 with WDR26 and ARMC8 were using N2a cells, and immunoblotting with TET2, WDR26 and ARMC8 antibody.

and *Tet2* KO N2a cell lines by using a CRISPR/Cas9 system. Western blots showed that TET2 level significantly increased in the *Armc8* KO and *Wdr26* KO cells (Fig. 6A and 6B), whereas the deletion of *Tet2* did not affect the expression levels of ARMC8 and WDR26 in the N2a cells (Fig. 6C). We further transfected ARMC8 or WDR26 overexpression plasmids to complement the deficiency in the *Armc8* KO or *Wdr26* KO cell lines. ARMC8 and WDR26 overexpression significantly decreased the level of TET2 ($P < 0.05$, 0.01, Fig. 6D–6G) but not the level of TET1 or TET3 (Fig. S2C and S2D). These results implied that TET2 is a novel downstream target of the GID E3 ligase complex during neuronal differentiation.

As GID complex is an enzyme with ubiquitin modification function, we subsequently explored the effect of the GID complex on TET2 ubiquitination. We examined the effect of the overexpression of the two core subunits of the GID complex on the ubiquitination of TET2 in N2a cells after the overexpression of HA-WDR26 or FLAG-ARMC8 plasmids. The results showed that ubiquitinated TET2 significantly increased after the overexpression of HA-WDR26 or FLAG-ARMC8 plasmid in the N2a cells (Fig. 6H and 6K). To further verify the effect of the GID complex on the protein stability of TET2, we treated the *Armc8* or *Wdr26* KO N2a cells with cycloheximide (CHX), which can block protein synthesis, for 0, 1, 2, 4 and 8 h, respectively. The results showed that the half-life period of TET2 protein was about 2 h under normal conditions, and the degradation of TET2 protein decreased significantly after *Wdr26* or *Armc8* KO (Fig. 6I, 6J, 6L and 6M). Taken

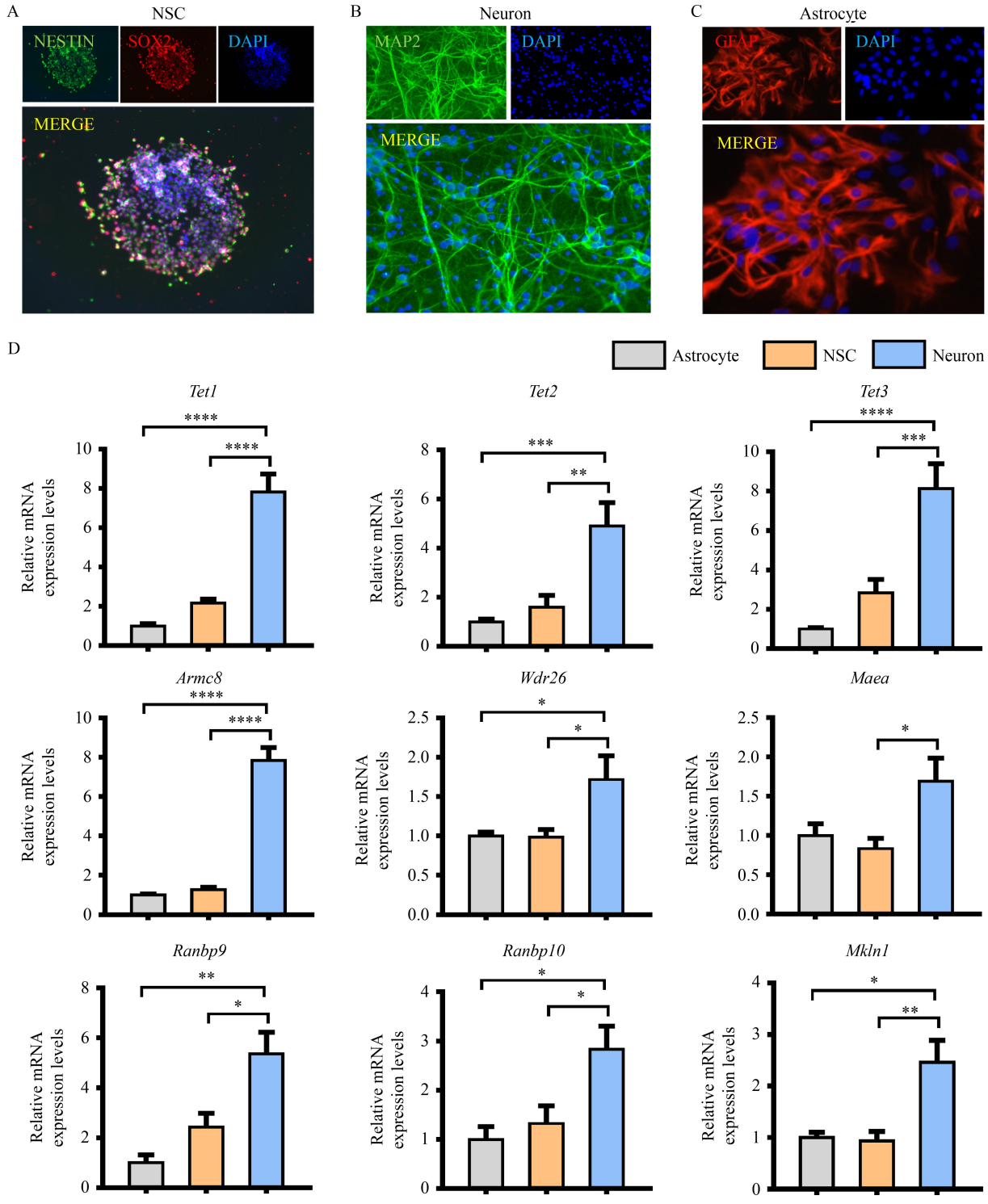

Fig. 4 TET2 and GID complex was highly expressed in neurons. (A–C) Representative images of SOX2$^+$ (red) and NESTIN$^+$ (green) NSC (A), MAP2$^+$ (green) neurons (B) and GFAP$^+$ (red) astrocytes (C). NSC and neurons were extracted from E14.5-day-old wild-type mice and astrocytes from 2-day-old mice. (D) Relative mRNA levels of TET family members and GID complex members in astrocytes, NSC, and neurons were examined; n = 5–6. Quantified data were normalized to the control group. The value was equal to 1. All data were presented as mean ± SEM. One-way ANOVA was used. *P < 0.05; **P < 0.01; ***P < 0.001; ****P < 0.0001.

together, the TET2 protein was more stable in the *Wdr26* or *Armc8* KO N2a cells.

In addition, *Wdr26* haploinsufficiency causes the Skraban-Deardorff syndrome characterized by developmental delay or intellectual disability, characteristic facial features, hypotonia, epilepsy, and infant feeding

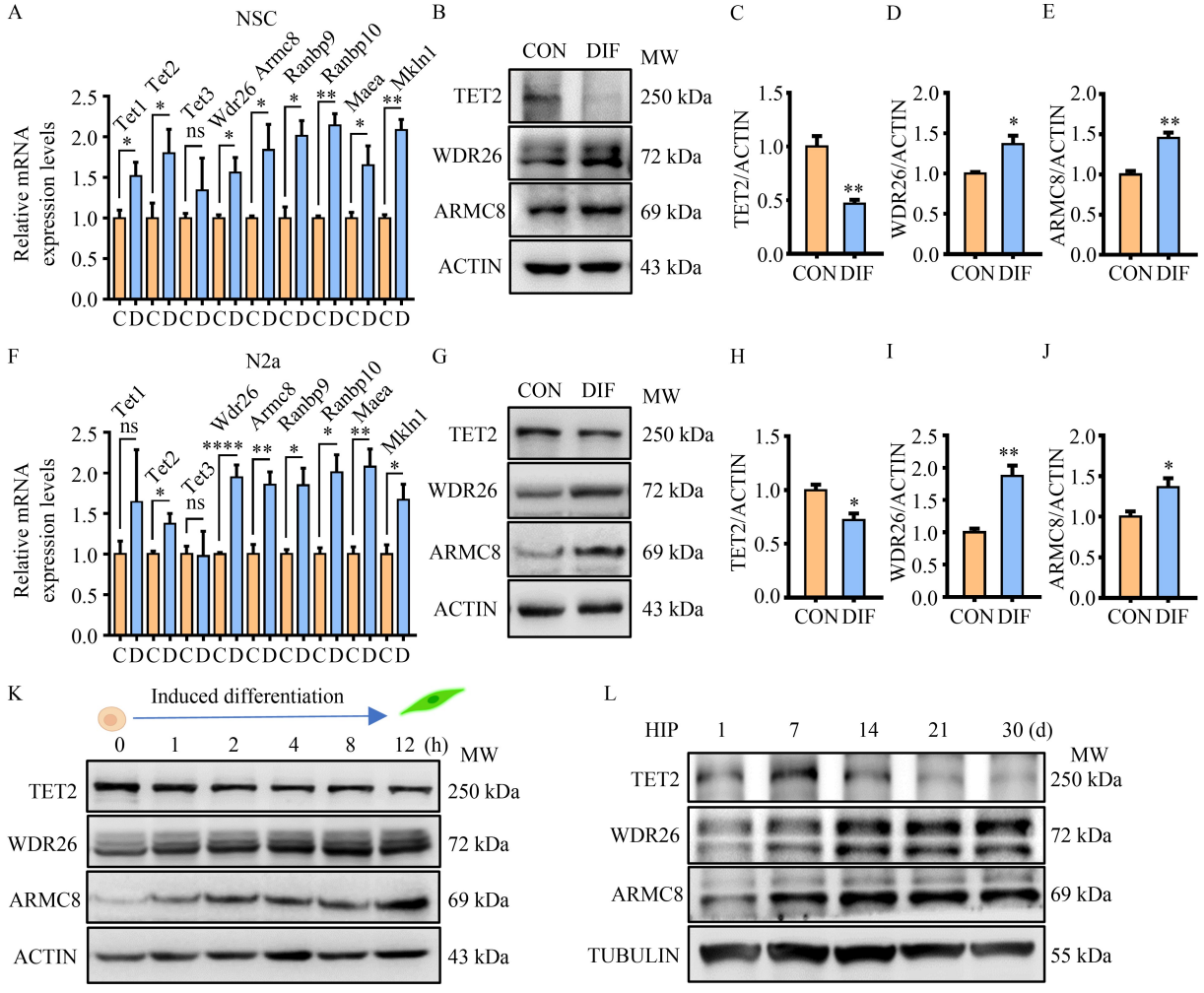

Fig. 5 TET2-GID complex is involved in neuronal differentiation. (A) RT-PCR of TET family and GID complex members' relative mRNA levels before and after NSC differentiation; $n = 4$. (B–E) Representative Western blots (B) and quantitative analysis of TET2 (C), WDR26 (D), and ARMC8 (E) in NSC before and after differentiation; $n = 4$. (F) RT-PCR of TET family and GID complex members' relative mRNA levels before and after N2a cell differentiation; $n = 4$. (G–J) Representative Western blots (G) and quantitative analysis of TET2 (H), WDR26 (I), and ARMC8 (J) in N2a cells before and after differentiation; $n = 4$. (K) Representative Western blots of TET2, WDR26, and ARMC8 during N2a differentiation. NSC differentiation was induced by forskolin (1 μmol/L) and RA (1 μmol/L) for 48 h, and N2a cell differentiation was induced by RA (20 μmol/L) for 12 h. (L) Representative Western blots of TET2, WDR26, and ARMC8 in the hippocampi of mice from days 1, 7, 14, 21, and 30. Quantified data were normalized to the control group, and the value was equal to 1. All data were presented as mean ± SEM. Unpaired two-tailed Student's *t*-test was used. $^{*}P < 0.05$; $^{**}P < 0.01$; $^{****}P < 0.0001$.

difficulties [18]. The mechanism by which *Wdr26* haploinsufficiency leads to these symptoms has yet to be elucidated. To determine whether TET2 stability is specifically regulated by the GID complex under physiologic conditions, we generated the heterozygous *Wdr26* knockout ($Wdr26^{+/-}$) mice (Fig. S1I and S1J). The Western blot results showed an increased expression of TET2 and no change in TET1 or TET3 expression in the prefrontal cortex of $Wdr26^{+/-}$ mice ($P < 0.05$, Fig. 7A–7D).

Armc8 or *Wdr26* KO affected the process of neuronal differentiation

To elucidate the function and biological significance of the GID complex in regulating the protein stability of TET2. We first examined the changes in 5hmC and 5mC after *Wdr26* or *Armc8* was knocked out in the N2a cells. Dot blot showed that the level of 5hmC in *Wdr26* or *Armc8* KO N2a cells significantly decreased, whereas the level of 5mC had no significant effect ($P < 0.05$, Fig. 8A–8F). Given the effect of TET2 on neuronal differentiation, we induced the differentiation of *Wdr26* or *Armc8* knockout N2a cells and examined the effect of the GID complex key subunit deficiency on neuronal differentiation. The results showed that *Armc8* or *Wdr26* KO significantly increased the differentiation ratio of the N2a cells (Fig. 9A). The *Wdr26* KO N2a cells had a higher proportion of differentiation and longer synapses

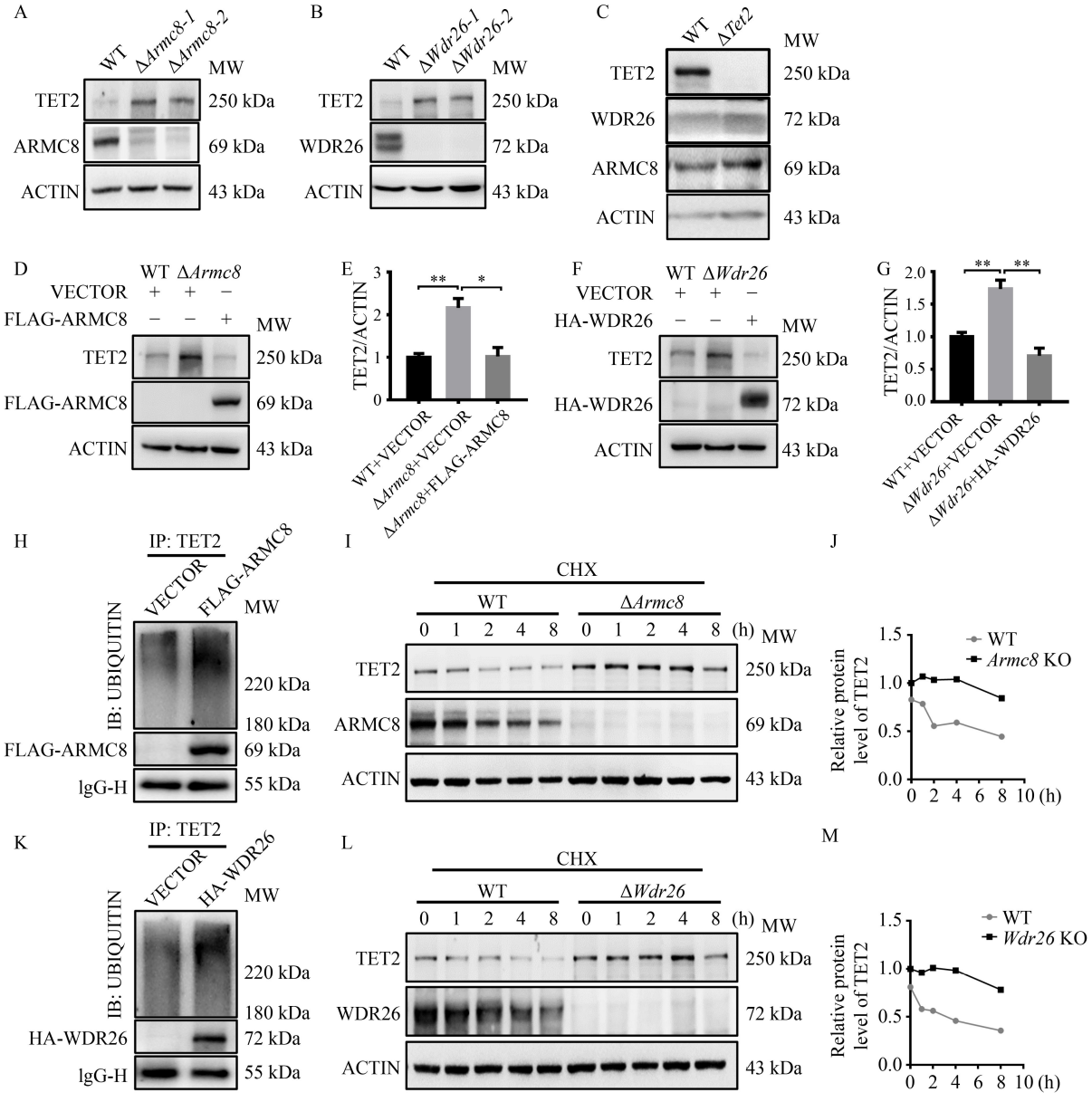

Fig. 6 TET2 is the direct substrate of the GID complex. (A–C) Western blots confirmed the knockout of *Armc8* (A), *Wdr26* (B), or *Tet2* (C) by sgRNAs in the N2a cells. (D,E) A rescue experiment was used to detect the effect of *Armc8* KO on the degradation of TET2 with overexpression FLAG-ARMC8 plasmids in the *Armc8* KO N2a cells. Wild-type (WT) N2a cells were transfected with vector plasmids (the first lane), and *Armc8* KO N2a cells were transfected with vector or FLAG-ARMC8 plasmids (the second and third lanes). Representative Western blots (D) and quantitative analysis of TET2 and FLAG-ARMC8 (E); $n = 3$. (F,G) WT N2a cells were transfected with vector plasmids (the first lane), and the *Wdr26* KO N2a cells were transfected with vector or HA-WDR26 plasmids (the second and third lanes). Representative Western blots (F) and quantitative analysis of TET2 and HA-WDR26 (G) with overexpression HA-WDR26 plasmids in the *Wdr26* KO N2a cells; $n = 3$. (H) Representative Western blots of TET2 ubiquitination of control or ARMC8-overexpressed N2a cells. (I,J) Representative Western blots (I) and quantitative analysis (J) of control or *Armc8* KO N2a cells, which were treated with 25 μg/mL cycloheximide (CHX) for different periods. (K) Representative Western blots of TET2 ubiquitination of control or WDR26-overexpressed N2a cells. (L,M) Representative Western blots (L) and quantitative analysis (M) of control or *Wdr26*-knockout N2a cells treated with 25 μg/mL CHX for different periods. (I, J, L and M) WT or *Armc8* (I,J) or *Wdr26* (L,M) knockout N2a cells were treated with 25 μg/mL CHX for different periods. The levels of the indicated proteins were examined by immunoblotting. Quantified data were normalized to the control group, and the value was equal to 1. All data were presented as mean ± SEM. One-way ANOVA was used. *$P < 0.05$; **$P < 0.01$.

($P < 0.0001$, 0.01, Fig. 9B and 9C). We knocked down *Wdr26* or *Armc8* in NSC derived from WT or *Tet2* cKO mice (Fig. 9D and 9F) and induced differentiation for 48 h. RT-PCR results showed that the reduction of *Armc8* and *Wdr26* increased the expression level of TUJ1 after WT NSC differentiation but not NSC from the *Tet2* cKO mice (Fig. 9E and 9G). In conclusion, these results suggested that the GID complex can regulate the level of

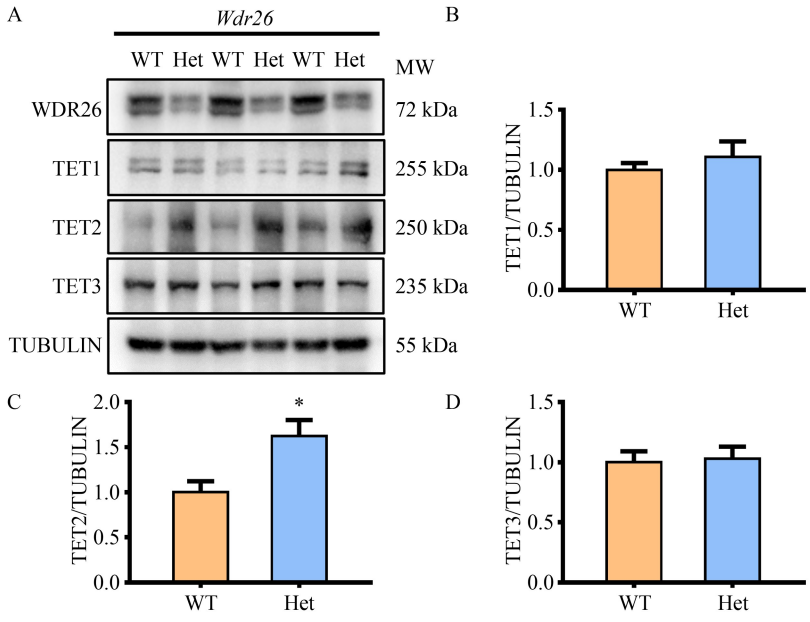

Fig. 7 TET2 protein increased in *Wdr26* heterozygous knockout mice. (A–D) Representative Western blots (A) and quantitative analysis of TET1 (B), TET2 (C), and TET3 (D) in wild-type and *Wdr26* heterozygous knockout mice; $n = 3$. Quantified data were normalized to the control group, and the value was equal to 1. All data were presented as mean ± SEM. Unpaired two-tailed Student's *t*-test was used. $^*P < 0.05$.

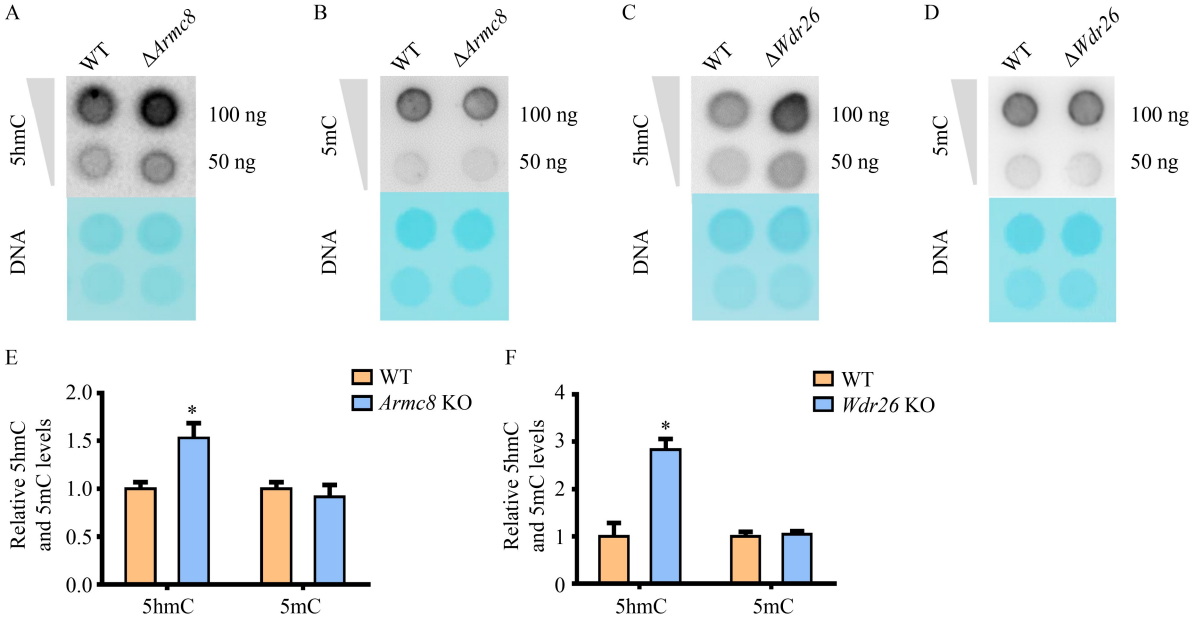

Fig. 8 GID complex subunit deletion promotes the DNA 5-hydroxymethylation. (A,B and E) Representative 5hmC (A) and 5mC (B) dot blots and quantitative analysis (E) of wild-type (WT) and *Armc8* KO N2a cells; $n = 3$. (C,D and F) Representative 5hmC (C) and 5mC (D) dot blots and quantitative analysis (F) of WT and *Wdr26* KO N2a cells; $n = 3$. Quantified data were normalized to the control group, and the value was equal to 1. All data were presented as mean ± SEM. Two-way ANOVA was used. $^*P < 0.05$.

5hmC and further influence the differentiation of nerve cells by regulating the level of TET2.

Discussion

Here, the critical finding presented is the discovery of the GID complex, a new regulatory factor that regulates the stability of TET2. The GID complex involves neuronal differentiation homeostasis by regulating the protein level of TET2. As the focus of neurological disorders, stem cells need to undergo a rigorous and dynamic gene expression regulation for the determination of the

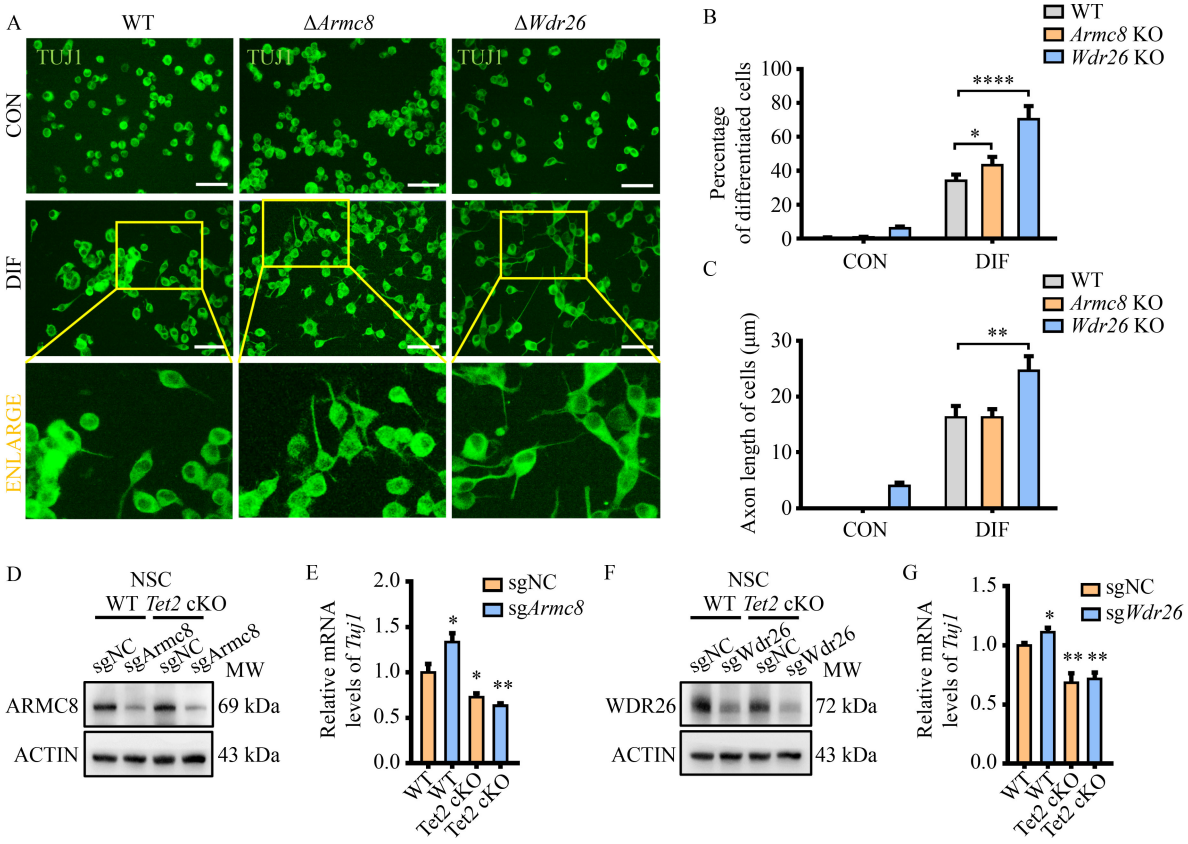

Fig. 9 GID complex subunit deletion promoted the process of neuronal differentiation. (A) Representative images of wild-type (WT), *Armc8* KO, and *Wdr26* KO N2a cells before and after differentiation. (B,C) Percentage of differentiated cells (B) and axon length (C) of N2a cells of WT and *Wdr2*6 KO N2a cells; $n = 3$. (D, F) Western blots confirmed the knockdown of *Armc8* (D) and *Wdr2*6 (F) by sgRNAs in NSC. (E,G) RT-PCR of *Tuj1* mRNA level of *Armc8* (E) and *Wdr26* (G) knockdown NSC after induced differentiation; $n = 4$. Quantified data were normalized to the control group, and the value was equal to 1. All data were presented as mean ± SEM. Unpaired two-tailed Student's *t*-test (E,G) and two-way ANOVA (B,C) were used. *$P < 0.05$; **$P < 0.01$.

maintenance and development of different organs [27,28]. Similarly, in the nervous system, NSC must carefully balance self-renewal and differentiation to maintain brain homeostasis and ensure the proper number of differentiated cell types needed to keep brain balance [29]. NSC undergo symmetric division to ensure self-renewal and asymmetric division to pre-differentiate [30]. The dys-differentiation or excessive self-renewal of NSC can lead to microcephaly [31] and brain tumor [32]. The premature differentiation of neurons may result in the insufficient pool reserve of neural progenitor cells and unbalanced distribution of other types of nerve cells, impede nerve cell migration, and impair the projection of brain regions [29]. The transformation of NSC into other types of nerve cells is determined by many stem cell regulatory factors, including SOX2, NOTCH1, CYCLIN-B1, CYCLIN-D1, and MYT1 [27]. Many genes, such as *Foxg1* [33], *Mcph1* [34], and *Nox* [35], affect brain development abnormalities or neuropsychiatric disorders caused by neural differentiation. Thus, many molecular mechanisms that influence neuronal differentiation need to be explored.

As an important member of epigenetic regulatory enzymes, the TET family promotes DNA demethylation by catalyzing DNA 5mC to 5hmC, 5-formylcytosine, and 5-carboxyl cytosine [1]. All TET family members participate in neural differentiation in nonoverlapping roles. *Tet3* KO ESCs can be induced to differentiate into neural progenitors, they undergo rapid apoptosis and show greatly compromised terminal differentiation [6]. Tet1 deficiency diminishes the adult SGZ neural progenitor pool but has no significant effect on the generation of neurons, astrocytes, and oligodendrocytes [36]. Our results showed TET2 inhibits the differentiation of NSC into neurons. Understanding how different TET enzymes act on 5mC of specific-target genes for the cell specificity and functional specificity of different TET enzymes is necessary. This function may be mediated by recruiting additional chaperone proteins or upstream molecular regulation. In the exploration for the role of TET2 in neural differentiation, we first detected the expression of TET2 before and after neuronal differentiation. However, the function of one gene often depends on the actual protein output. After

differentiation, the expression of *Tet2* mRNA was upregulated, whereas the level of TET2 protein was downregulated. For this normal physiologic process of neuronal differentiation, we will explore in greater depth the significance of decreased levels of TET2 in neuronal differentiation.

Current studies on the protein regulation of TET2 focus on the apoptosis, calpeptin, and ubiquitin degradation pathway. We found that proteasome has the most significant effect on the level of TET2 in nerve cells. By performing a co-immunoprecipitation/MS assay, we found that the GID complex physically interacts with and involves in the regulation of the stability of TET2. The GID complex regulates the cell cycle but has not been studied comprehensively in the CNS. Interestingly, GID subunits are involved in the development of many diseases related to neural differentiation, for example, the Skraban-Deardorff syndrome, a disease related to variations in *Wdr26* gene and characterized by a combination of symptoms: intellectual disability, seizures, abnormal gait, and distinctive facial features [18]. Our results showed an increased expression of TET2 but no change in TET1 or TET3 in the *Wdr26* heterozygous recombinant mice. Whether this disease is related to TET2-induced changes in global 5hmC level in Skraban-Deardorff syndrome will be further investigated as many clinical features of this disease overlap with "transcriptomopathies" [37]. Moreover, *Xenopus* NSC *Armc8* knockout promotes neuronal differentiation [38]. *Mkln1* mutations may increase the risk of bipolar disorder [39]. Given these close relationships, we investigated the effect of the GID complex on the expression of TET2 protein in neurons. In fact, the GID complex is strongly associated with many other diseases, such as cancer, which cause over 60% of tumor cases to show alterations in CTLH gene expression [40]. These mechanisms are unclear. Therefore, further investigation is needed to examine whether the GID complex-TET2 axis plays a similar regulatory role in other cell types. In addition, we plan to investigate the regulatory role of the GID complex on TET2 in neuronal differentiation into diseases related to neuronal differentiation. We hope to find conditions that would use GID-TET2 as the potential target and provide insights into treatment strategies for these patients.

Acknowledgements

We thank Professor Caiyong Chen from College of Life Sciences, Zhejiang University for providing the FLAG-ARMC8 and FLAG-WDR26 plasmids. This study was supported by the National Science Foundation of China (Nos. 82071511 and 81120108011), National Key R&D Program of China (No. 2017YFE0103700), Shandong Provincial Natural Science Foundation (No. ZR2019ZD32), the Priority Academic Program Development of Jiangsu Higher Education Institutions, and Postgraduate Research & Practice Innovation Program of Jiangsu Province (No. KYCX21_2974).

Compliance with ethics guidelines

Conflicts of interest Meiling Xia, Rui Yan, Wenjuan Wang, Meng Zhang, Zhigang Miao, Bo Wan, and Xingshun Xu declare that they have no competing interests.

All animal use protocols were approved by the institutional animal care and use committee of Soochow University. All institutional and national guidelines for the care and use of laboratory animals were followed.

Electronic Supplementary Material Supplementary material is available in the online version of this article at https://doi.org/10.1007/s11684-023-1007-9 and is accessible for authorized users.

References

1. Ito S, Shen L, Dai Q, Wu SC, Collins LB, Swenberg JA, He C, Zhang Y. Tet proteins can convert 5-methylcytosine to 5-formylcytosine and 5-carboxylcytosine. Science 2011; 333(6047): 1300–1303
2. He YF, Li BZ, Li Z, Liu P, Wang Y, Tang Q, Ding J, Jia Y, Chen Z, Li L, Sun Y, Li X, Dai Q, Song CX, Zhang K, He C, Xu GL. Tet-mediated formation of 5-carboxylcytosine and its excision by TDG in mammalian DNA. Science 2011; 333(6047): 1303–1307
3. Wu X, Zhang Y. TET-mediated active DNA demethylation: mechanism, function and beyond. Nat Rev Genet 2017; 18(9): 517–534
4. Koh KP, Yabuuchi A, Rao S, Huang Y, Cunniff K, Nardone J, Laiho A, Tahiliani M, Sommer CA, Mostoslavsky G, Lahesmaa R, Orkin SH, Rodig SJ, Daley GQ, Rao A. Tet1 and Tet2 regulate 5-hydroxymethylcytosine production and cell lineage specification in mouse embryonic stem cells. Cell Stem Cell 2011; 8(2): 200–213
5. Dawlaty MM, Ganz K, Powell BE, Hu YC, Markoulaki S, Cheng AW, Gao Q, Kim J, Choi SW, Page DC, Jaenisch R. Tet1 is dispensable for maintaining pluripotency and its loss is compatible with embryonic and postnatal development. Cell Stem Cell 2011; 9(2): 166–175
6. Li T, Yang D, Li J, Tang Y, Yang J, Le W. Critical role of Tet3 in neural progenitor cell maintenance and terminal differentiation. Mol Neurobiol 2015; 51(1): 142–154
7. Li X, Yao B, Chen L, Kang Y, Li Y, Cheng Y, Li L, Lin L, Wang Z, Wang M, Pan F, Dai Q, Zhang W, Wu H, Shu Q, Qin Z, He C, Xu M, Jin P. Ten-eleven translocation 2 interacts with forkhead box O3 and regulates adult neurogenesis. Nat Commun 2017; 8: 15903
8. Zhang Q, Hu Q, Wang J, Miao Z, Li Z, Zhao Y, Wan B, Allen EG, Sun M, Jin P, Xu X. Stress modulates Ahi1-dependent nuclear localization of ten-eleven translocation protein 2. Hum Mol Genet 2021; 30(22): 2149–2160
9. Li L, Miao M, Chen J, Liu Z, Li W, Qiu Y, Xu S, Wang Q. Role of Ten eleven translocation-2 (Tet2) in modulating neuronal

morphology and cognition in a mouse model of Alzheimer's disease. J Neurochem 2021; 157(4): 993–1012
10. Mi Y, Gao X, Dai J, Ma Y, Xu L, Jin W. A Novel function of TET2 in CNS: sustaining neuronal survival. Int J Mol Sci 2015; 16(9): 21846–21857
11. Wang Y, Zhang Y. Regulation of TET protein stability by calpains. Cell Rep 2014; 6(2): 278–284
12. Cheng J, Guo S, Chen S, Mastriano SJ, Liu C, D'Alessio AC, Hysolli E, Guo Y, Yao H, Megyola CM, Li D, Liu J, Pan W, Roden CA, Zhou XL, Heydari K, Chen J, Park IH, Ding Y, Zhang Y, Lu J. An extensive network of TET2-targeting microRNAs regulates malignant hematopoiesis. Cell Rep 2013; 5(2): 471–481
13. Wu D, Hu D, Chen H, Shi G, Fetahu IS, Wu F, Rabidou K, Fang R, Tan L, Xu S, Liu H, Argueta C, Zhang L, Mao F, Yan G, Chen J, Dong Z, Lv R, Xu Y, Wang M, Ye Y, Zhang S, Duquette D, Geng S, Yin C, Lian CG, Murphy GF, Adler GK, Garg R, Lynch L, Yang P, Li Y, Lan F, Fan J, Shi Y, Shi YG. Glucose-regulated phosphorylation of TET2 by AMPK reveals a pathway linking diabetes to cancer. Nature 2018; 559(7715): 637–641
14. Ko M, An J, Bandukwala HS, Chavez L, Aijö T, Pastor WA, Segal MF, Li H, Koh KP, Lähdesmäki H, Hogan PG, Aravind L, Rao A. Modulation of TET2 expression and 5-methylcytosine oxidation by the CXXC domain protein IDAX. Nature 2013; 497(7447): 122–126
15. Lv L, Wang Q, Xu Y, Tsao LC, Nakagawa T, Guo H, Su L, Xiong Y. Vpr targets TET2 for degradation by $CRL4^{VprBP}$ E3 ligase to sustain IL-6 expression and enhance HIV-1 replication. Mol Cell 2018; 70(5): 961–970.e5
16. Santt O, Pfirrmann T, Braun B, Juretschke J, Kimmig P, Scheel H, Hofmann K, Thumm M, Wolf DH. The yeast GID complex, a novel ubiquitin ligase (E3) involved in the regulation of carbohydrate metabolism. Mol Biol Cell 2008; 19(8): 3323–3333
17. Lampert F, Stafa D, Goga A, Soste MV, Gilberto S, Olieric N, Picotti P, Stoffel M, Peter M. The multi-subunit GID/CTLH E3 ubiquitin ligase promotes cell proliferation and targets the transcription factor Hbp1 for degradation. eLife 2018; 7: e35528
18. Skraban CM, Wells CF, Markose P, Cho MT, Nesbitt AI, Au PYB, Begtrup A, Bernat JA, Bird LM, Cao K, de Brouwer APM, Denenberg EH, Douglas G, Gibson KM, Grand K, Goldenberg A, Innes AM, Juusola J, Kempers M, Kinning E, Markie DM, Owens MM, Payne K, Person R, Pfundt R, Stocco A, Turner CLS, Verbeek NE, Walsh LE, Warner TC, Wheeler PG, Wieczorek D, Wilkens AB, Zonneveld-Huijssoon E; Deciphering Developmental Disorders Study; Kleefstra T, Robertson SP, Santani A, van Gassen KLI, Deardorff MA. WDR26 haploinsufficiency causes a recognizable syndrome of intellectual disability, seizures, abnormal gait, and distinctive facial features. Am J Hum Genet 2017; 101(1): 139–148
19. Córdova-Palomera A, Fatjó-Vilas M, Gastó C, Navarro V, Krebs MO, Fañanás L. Genome-wide methylation study on depression: differential methylation and variable methylation in monozygotic twins. Transl Psychiatry 2015; 5(4): e557
20. Tangsuwansri C, Saeliw T, Thongkorn S, Chonchaiya W, Suphapeetiporn K, Mutirangura A, Tencomnao T, Hu VW, Sarachana T. Investigation of epigenetic regulatory networks associated with autism spectrum disorder (ASD) by integrated global LINE-1 methylation and gene expression profiling analyses. PLoS One 2018; 13(7): e0201071
21. Dong C, Zhang H, Li L, Tempel W, Loppnau P, Min J. Molecular basis of GID4-mediated recognition of degrons for the Pro/N-end rule pathway. Nat Chem Biol 2018; 14(5): 466–473
22. Zhang YW, Wang Z, Xie W, Cai Y, Xia L, Easwaran H, Luo J, Yen RC, Li Y, Baylin SB. Acetylation enhances TET2 function in protecting against abnormal DNA methylation during oxidative stress. Mol Cell 2017; 65(2): 323–335
23. Guallar D, Bi X, Pardavila JA, Huang X, Saenz C, Shi X, Zhou H, Faiola F, Ding J, Haruehanroengra P, Yang F, Li D, Sanchez-Priego C, Saunders A, Pan F, Valdes VJ, Kelley K, Blanco MG, Chen L, Wang H, Sheng J, Xu M, Fidalgo M, Shen X, Wang J. RNA-dependent chromatin targeting of TET2 for endogenous retrovirus control in pluripotent stem cells. Nat Genet 2018; 50(3): 443–451
24. Sun Z, Smrcka AV, Chen S. WDR26 functions as a scaffolding protein to promote Gβγ-mediated phospholipase C β2 (PLCβ2) activation in leukocytes. J Biol Chem 2013; 288(23): 16715–16725
25. Chen SJ, Wu X, Wadas B, Oh JH, Varshavsky A. An N-end rule pathway that recognizes proline and destroys gluconeogenic enzymes. Science 2017; 355(6323): eaal3655
26. Hochgerner H, Zeisel A, Lönnerberg P, Linnarsson S. Conserved properties of dentate gyrus neurogenesis across postnatal development revealed by single-cell RNA sequencing. Nat Neurosci 2018; 21(2): 290–299
27. Muhr J, Hagey DW. The cell cycle and differentiation as integrated processes: cyclins and CDKs reciprocally regulate Sox and Notch to balance stem cell maintenance. BioEssays 2021; 43(7): e2000285
28. Borlongan CV. Regenerative medicine during the pandemic period. Brain Circ 2021; 7(1): 1–2
29. Farkas LM, Huttner WB. The cell biology of neural stem and progenitor cells and its significance for their proliferation versus differentiation during mammalian brain development. Curr Opin Cell Biol 2008; 20(6): 707–715
30. Guo Z, Chen M, Chao Y, Cai C, Liu L, Zhao L, Li L, Bai QR, Xu Y, Niu W, Shi L, Bi Y, Ren D, Yuan F, Shi S, Zeng Q, Han K, Shi Y, Bian S, He G. RGCC balances self-renewal and neuronal differentiation of neural stem cells in the developing mammalian neocortex. EMBO Rep 2021; 22(9): e51781
31. Gilmore EC, Walsh CA. Genetic causes of microcephaly and lessons for neuronal development. Wiley Interdiscip Rev Dev Biol 2013; 2(4): 461–478
32. Groszer M, Erickson R, Scripture-Adams DD, Dougherty JD, Le Belle J, Zack JA, Geschwind DH, Liu X, Kornblum HI, Wu H. PTEN negatively regulates neural stem cell self-renewal by modulating G0-G1 cell cycle entry. Proc Natl Acad Sci USA 2006; 103(1): 111–116
33. Wilpert NM, Marguet F, Maillard C, Guimiot F, Martinovic J, Drunat S, Attié-Bitach T, Razavi F, Tessier A, Capri Y, Laquerrière A, Bahi-Buisson N. Human neuropathology confirms projection neuron and interneuron defects and delayed oligodendrocyte production and maturation in FOXG1 syndrome. Eur J Med Genet 2021; 64(9): 104282
34. Gruber R, Zhou Z, Sukchev M, Joerss T, Frappart PO, Wang ZQ. MCPH1 regulates the neuroprogenitor division mode by coupling the centrosomal cycle with mitotic entry through the Chk1-Cdc25 pathway. Nat Cell Biol 2011; 13(11): 1325–1334
35. Maraldi T, Angeloni C, Prata C, Hrelia S. NADPH oxidases: redox

regulators of stem cell fate and function. antioxidants 2021; 10(6): 973

36. Zhang RR, Cui QY, Murai K, Lim YC, Smith ZD, Jin S, Ye P, Rosa L, Lee YK, Wu HP, Liu W, Xu ZM, Yang L, Ding YQ, Tang F, Meissner A, Ding C, Shi Y, Xu GL. Tet1 regulates adult hippocampal neurogenesis and cognition. Cell Stem Cell 2013; 13(2): 237–245
37. Izumi K. Disorders of transcriptional regulation: an emerging category of multiple malformation syndromes. Mol Syndromol 2016; 7(5): 262–273
38. Bestman JE, Huang LC, Lee-Osbourne J, Cheung P, Cline HT. An *in vivo* screen to identify candidate neurogenic genes in the developing *Xenopus* visual system. Dev Biol 2015; 408(2): 269–291
39. Nassan M, Li Q, Croarkin PE, Chen W, Colby CL, Veldic M, McElroy SL, Jenkins GD, Ryu E, Cunningham JM, Leboyer M, Frye MA, Biernacka JM. A genome wide association study suggests the association of muskelin with early onset bipolar disorder: implications for a GABAergic epileptogenic neurogenesis model. J Affect Disord 2017; 208: 120–129
40. Huffman N, Palmieri D, Coppola V. The CTLH complex in cancer cell plasticity. J Oncol 2019; 2019: 4216750